

Article

Antimicrobial Activity of a Titanium Dioxide Additivated Thermoset

Markus Ahrens ^{1,*} , Theresa Fischer ¹, Nina Zuber ¹, Serhiy Yatsenko ², Thomas Hochrein ², Martin Bastian ², Markus Eblenkamp ³ and Petra Mela ¹

¹ Chair of Medical Materials and Implants, Department of Mechanical Engineering, TUM School of Engineering and Design, Munich Institute of Biomedical Engineering, Technical University of Munich, Boltzmannstr. 15, 85748 Garching, Germany; theresa.fischer@tum.de (T.F.); nina.zuber@tum.de (N.Z.); petra.mela@tum.de (P.M.)

² SKZ—German Plastics Center, Friedrich-Bergius-Ring 22, 97076 Würzburg, Germany; s.yatsenko@skz.de (S.Y.); t.hochrein@skz.de (T.H.); m.bastian@skz.de (M.B.)

³ TUM School of Engineering and Design, Technical University of Munich, Lichtenbergstr. 4a, 85748 Garching, Germany; markus.eblenkamp@tum.de

* Correspondence: markus.ahrens@tum.de

Abstract: The transmission of pathogens via surfaces poses a major health problem, particularly in hospital environments. Antimicrobial surfaces can interrupt the path of spread, while photocatalytically active titanium dioxide (TiO₂) nanoparticles have emerged as an additive for creating antimicrobial materials. Irradiation of such particles with ultraviolet (UV) light leads to the formation of reactive oxygen species that can inactivate bacteria. The aim of this research was to incorporate TiO₂ nanoparticles into a cellulose-reinforced melamine-formaldehyde resin (MF) to obtain a photocatalytic antimicrobial thermoset, to be used, for example, for device enclosures or tableware. To this end, composites of MF with 5, 10, 15, and 20 wt% TiO₂ were produced by ultrasonication and hot pressing. The incorporation of TiO₂ resulted in a small decrease in tensile strength and little to no decrease in Shore D hardness, but a statistically significant decrease in the water contact angle. After 48 h of UV irradiation, a statistically significant decrease in tensile strength for samples with 0 and 10 wt% TiO₂ was measured but with no statistically significant differences in Shore D hardness, although a statistically significant increase in surface hydrophilicity was measured. Accelerated methylene blue (MB) degradation was measured during a further 2.5 h of UV irradiation and MB concentrations of 12% or less could be achieved. Samples containing 0, 10, and 20 wt% TiO₂ were investigated for long-term UV stability and antimicrobial activity. Fourier-transform infrared spectroscopy revealed no changes in the chemical structure of the polymer, due to the incorporation of TiO₂, but changes were detected after 500 h of irradiation, indicating material degradation. Specimens pre-irradiated with UV for 48 h showed a total reduction in *Escherichia coli* when exposed to UV irradiation.

Keywords: MELOPAS[®] MF 152.7; AEROXIDE[®] TiO₂ P25; melamine-formaldehyde resin; titanium dioxide; UV irradiation; antimicrobial surface; photocatalytic effect; radical oxygen species; nosocomial infections



Citation: Ahrens, M.; Fischer, T.; Zuber, N.; Yatsenko, S.; Hochrein, T.; Bastian, M.; Eblenkamp, M.; Mela, P. Antimicrobial Activity of a Titanium Dioxide Additivated Thermoset. *Catalysts* **2022**, *12*, 829. <https://doi.org/10.3390/catal12080829>

Academic Editors: Biljana F. Abramovic and Tamara B. Ivetić

Received: 31 December 2021

Accepted: 24 July 2022

Published: 28 July 2022

Publisher's Note: MDPI stays neutral with regard to jurisdictional claims in published maps and institutional affiliations.



Copyright: © 2022 by the authors. Licensee MDPI, Basel, Switzerland. This article is an open access article distributed under the terms and conditions of the Creative Commons Attribution (CC BY) license (<https://creativecommons.org/licenses/by/4.0/>).

1. Introduction

Bacteria are present in all areas of daily life that can cause potentially dangerous infections [1]. The number of hospital-acquired infections (HAIs) in Germany can reach up to 600,000 cases per year, with up to 15,000 resulting in the death of the patient [2]. The transmission of hazardous microorganisms from a contaminated hospital surface to a patient either directly or through medical staff is a serious issue, but it can be disrupted by the use of antimicrobial surfaces [3,4].

Such surfaces can be created, for example, by applying coatings containing silver or copper nanoparticles or through incorporation of such particles [5–8]. Another promising approach is to use light-active photosensitizers such as nanoscale titanium dioxide (TiO₂) in

combination with ultraviolet (UV) irradiation of the surface, which leads to the formation of reactive oxygen species (ROS) that are able to kill adhering bacteria [9–14]. The current COVID-19 pandemic has demonstrated the importance of antimicrobial surfaces in the fight against pathogens, and initial studies have shown that TiO₂ nanoparticles are able to inactivate SARS-CoV-2 [15–18].

There are several theories concerning the unspecific site of action and the mechanism of interaction and killing of microorganisms by TiO₂. An attack on the bacteria can be brought about, for example, by the ROS inhibiting cell respiration or damaging the outer membrane [19]. Once the cell wall and membrane have been destroyed, the ROS can penetrate a germ's interior and arbitrarily destroy organic compounds. Damage to lipid radicals, coenzymes A or deoxyribonucleic acid (DNA), for example, results in cell lysis [20,21]. This varied attack means that germs are spontaneously combated from different sites of action [19]. This benefits the fight against microorganisms through antibiotics, which often act selectively on a single component of the bacterium [19,21,22].

Photoinduced superhydrophilicity can further increase the self-cleaning effect of the surface [12]. However, the same ROS can also impact the polymer matrix and bring about its degradation [23,24]. In some cases, this mechanism is exploited to increase the degradation rate and reduce plastic waste by introducing TiO₂ as an additive [22,24–26].

Coatings can be used to tailor surface properties. These include corrosion/wear resistance, hardness, texture, thermal/electrical insulation, wettability, hydrophobicity, and antimicrobial activity [27–29]. However, the durability of the coatings may be limited by thermal effects (deformation, cracks, delamination, etc.) or loose atmospheric protection (e.g., penetration of inclusions or contaminations in the substrate) [28]. The long-term antimicrobial property of coatings can be negatively influenced by chain cleavage, mechanical weakness, oxidative degradation, lack of adhesion to the substrate, or high surface reactivity, leading to surface conditioning [30]. The loss of the antimicrobial effect in the case of surface damage is a particular aspect of coatings that needs to be considered. To avoid this problem, we recently proposed incorporating particles directly in the bulk of the polymer [31].

This study investigates the incorporation of nanoscale TiO₂ in a melamine-formaldehyde (MF) resin with the aim of developing a new antimicrobial material. MF is used, for example, for electrical insulation parts such as plugs, switches, lamp sockets, clamps, and switching elements, but also for eating and drinking utensils and handles for cooking appliances [32]. In public institutions such as hospitals, these contact surfaces are frequently exposed to human contact and can act as germ transmitters. The use of antimicrobial materials can interrupt the nosocomial infection loop and, in turn, pathogen transmission [3]. However, there have been very few, if any, reported efforts relating to the development of MF-based antimicrobial thermosets using TiO₂.

This study evaluates the mechanical and chemical properties of unirradiated and UV-irradiated samples, along with the associated photocatalytic activity and antimicrobial effect.

2. Results and Discussion

We produced samples of MELOPAS[®] MF 152.7 with up to 20 wt% TiO₂ particles according to the procedure described later.

2.1. Mechanical Properties

Figure 1 shows the tensile strengths and Shore D hardness values of both unirradiated samples and samples irradiated for 48 h.

The tensile strength of the non-additivated MF (MF_0) was 74.38 ± 4.21 MPa, which is higher than the value range of 40 to 60 MPa given in the manufacturer's specifications [32]. A decrease in tensile strength was observed as increasing amounts of additive were incorporated into the polymer, but it was only statistically significant for MF_20 ($p < 0.01$). Rigid

fillers can have an effect on the stress–strain behavior of polymer matrices and can reduce the tensile strength [33].

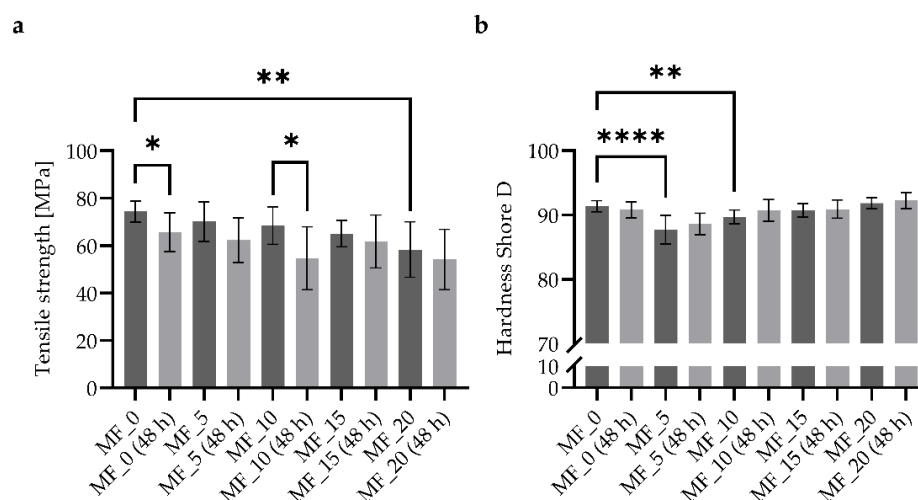


Figure 1. Effect of TiO₂ on mechanical properties. (a) Tensile strength of specimens unirradiated and irradiated for 48 h ($n = 8$); (b) Shore D hardness of unirradiated specimens and specimens irradiated for 48 h ($n = 3$, $i = 5$). * $p < 0.05$, ** $p < 0.01$, and **** $p < 0.0001$.

UV irradiation for 48 h caused the tensile strength to decrease in comparison with the unirradiated test specimens. Man et al. showed that the reduction in tensile strength of rutile-additivated polylactide (PLA) samples was smaller than that of pure PLA upon UV irradiation and with weight percentages of up to 3% [34]. The authors attributed the increased UV resistance to the UV screening effect of the particles. Our study produced similar results, although the MF_10 samples had a much higher particle content. This can be explained by the amount of rutile in the TiO₂ particles used in this study, which was only 10.6 wt% [35]. Overall, all the tensile strengths (unirradiated and 48 h UV-irradiated) measured were above or within the manufacturer's specifications (40 to 60 MPa for the MF) [32].

The Shore D hardness of MF_0 was 91.36 ± 0.83 . A small but statistically significant decrease was measured for MF_5 and MF_10. This contradicts the findings of Asiaban and Taghinejad, who showed that the Rockwell hardness of TiO₂ additivated acrylonitril-butadiene-styrene (ABS) decreased with increasing additive content. They attributed this to the formation of cavities around the particles during sample preparation [36].

For all filler contents, no statistically significant change ($p < 0.05$) in Shore D hardness was observed after UV irradiation. This could be due to the aforementioned UV screening effect of TiO₂, which could have a positive effect on the stability of MF [34].

2.2. Contact Angle Measurement

Figure 2 shows the contact angles of unirradiated and 48 h UV-irradiated samples. The contact angle of MF_0 was $88.41 \pm 5.50^\circ$ for distilled water. After incorporating TiO₂, the contact angle decreased statistically significantly ($p < 0.0001$) for all additivated specimens. UV irradiation for 48 h resulted in a further substantial, statistically significant reduction in the contact angles ($p < 0.0001$) compared to the unirradiated specimens, while no reduction was evident in the pure specimen (MF_0 (48 h)). With TiO₂ incorporated in the polymer and subsequent UV irradiation, the samples showed hydrophilic rather than hydrophobic properties. These results are in line with those reported by Sakai et al. [37]. In addition, Sakai et al. found that a minimum contact angle value was attained after a certain irradiation duration, and that this depended on the initial value of the contact angle. They found that increased UV intensity led to a faster decrease in the contact angle over the same period of time [37].

Overall, increased hydrophilicity due to UV irradiation of the additivated test specimens was a consequence of photocatalytically active TiO₂ nanoparticles.

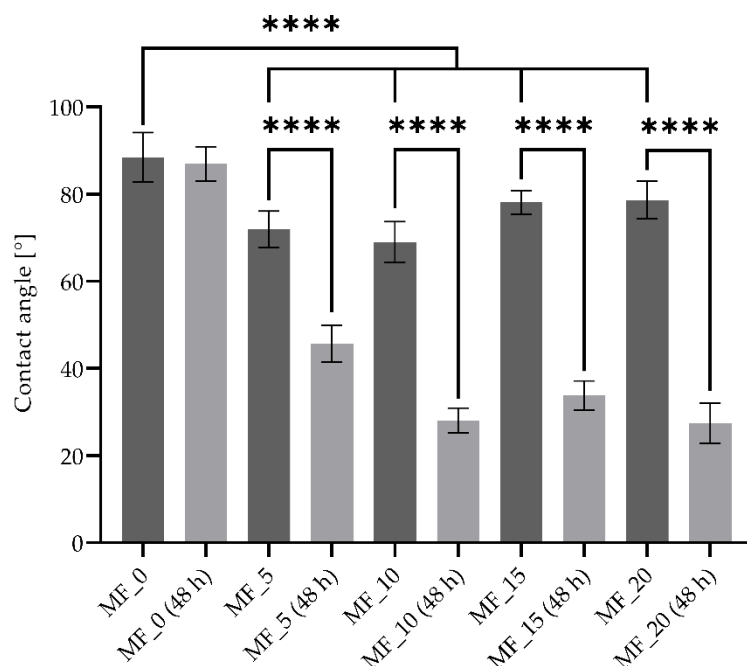


Figure 2. Effect of TiO₂ on contact angles of unirradiated and 48 h UV-irradiated samples ($n = 3$, $i = 5$). **** $p < 0.0001$.

2.3. Long-Term UV Stability

The samples were irradiated with UV light at an intensity of 50 W/m² for 500 h. The UV irradiation of the TiO₂ additivated samples led to a blue-grey discoloration of the surface, which intensified with increasing TiO₂ content due to the chalking cycle [38,39]. If not enough oxygen or water is available, Ti³⁺ cations can accumulate, resulting in a blue-gray discoloration. The absence of oxygen or water might be due to a polymer layer formed during production of the samples by hot pressing that enclosed the TiO₂ particles. Furthermore, irradiation of TiO₂ incorporated in a polymer can also lead to its degradation [23].

Fourier-transform infrared (FTIR) spectra were recorded for the test specimens in both unirradiated and irradiated states to detect possible chemical changes. Figure 3 shows the absorption spectra of unirradiated samples (MF_0, MF_10, and MF_20) and FTIR spectra for MF_0 (500 h) and MF_10 (500 h) after 500 h of UV irradiation. No FTIR spectrum could be recorded for irradiated MF_20 (500 h), as the sample had a highly porous surface, and the required contact pressure on the attenuated total reflection (ATR) unit could not be achieved.

The FTIR spectrum of MF_0 showed the expected pattern for an MF resin [40–42]. The additivated specimens MF_10 and MF_20 showed similar FTIR spectra, but the absorption peaks were lower than for MF_0. This could be due to the increased reflection of the IR rays as a result of the incorporated TiO₂ [41]. Moreover, Ti–O stretch bonds might have occurred in the additivated samples at wavenumbers below 800 cm^{−1} [43,44].

The peak at about 1700 cm^{−1} of MF_0 (500 h) and MF_10 (500 h) might be attributable to a carbonyl vibration and could indicate a degradation of the polymer, resulting, for example, in the generation of formaldehyde [45]. As this peak only occurred in samples irradiated with UV light, it might be concluded that this peak is independent of whether TiO₂ is added to the polymer and is due to the aging of MF caused by the UV irradiation. In addition, the peaks at 2850.3 cm^{−1} and 2917.8 cm^{−1}, which could indicate CH stretching vibrations, were not measured in the irradiated samples and could also be due to the influence of UV irradiation of the polymer.

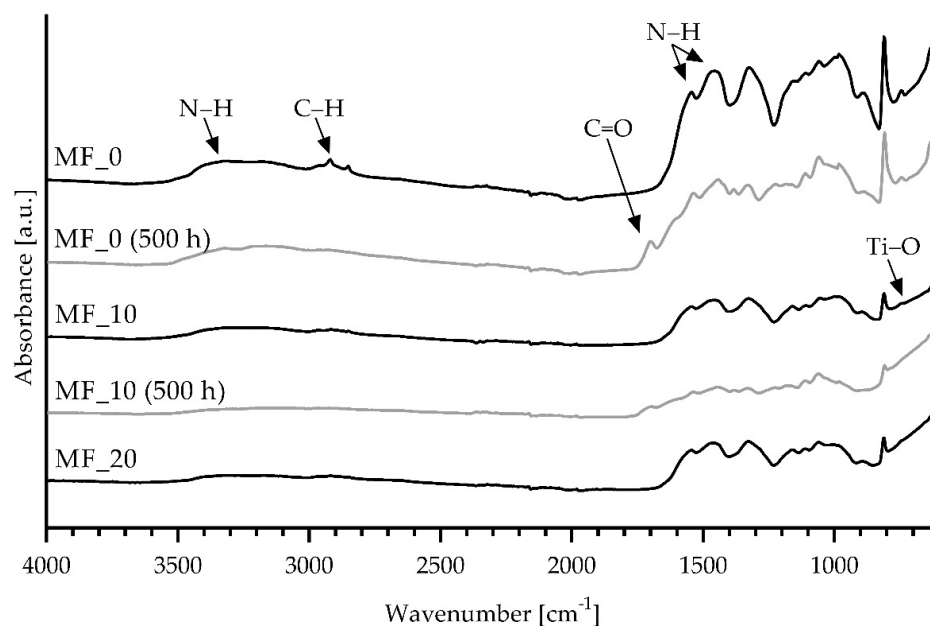


Figure 3. Effect of TiO₂ on the chemical structure of MF. FTIR spectra of nonirradiated samples MF_0, MF_10, and MF_20 and samples MF_0 (500 h) and MF_10 (500 h) irradiated for 500 h. No MF_20 (500 h) spectra could be recorded.

UV irradiation of the additivated sample might have led to a break in the NH bond [46] and the formation of ammonia (NH₃). This was observed in the reduced N–H absorption between 1480 and 1625 cm^{−1} as well as between 3120 and 3500 cm^{−1}.

2.4. Photocatalytic Activity

Photocatalytic activity of the different samples was estimated by the degradation of methylene blue (MB) [47].

Figure 4 shows the UV–Vis spectrum of MB along with spectra of an MB solution degraded by UV irradiation of TiO₂ particles in the solution after 5 and 10 min. After 10 min, an almost complete degradation of MB was observed, resulting in an MB content of $1.55 \pm 1.77\%$, as determined by optical density measurements.

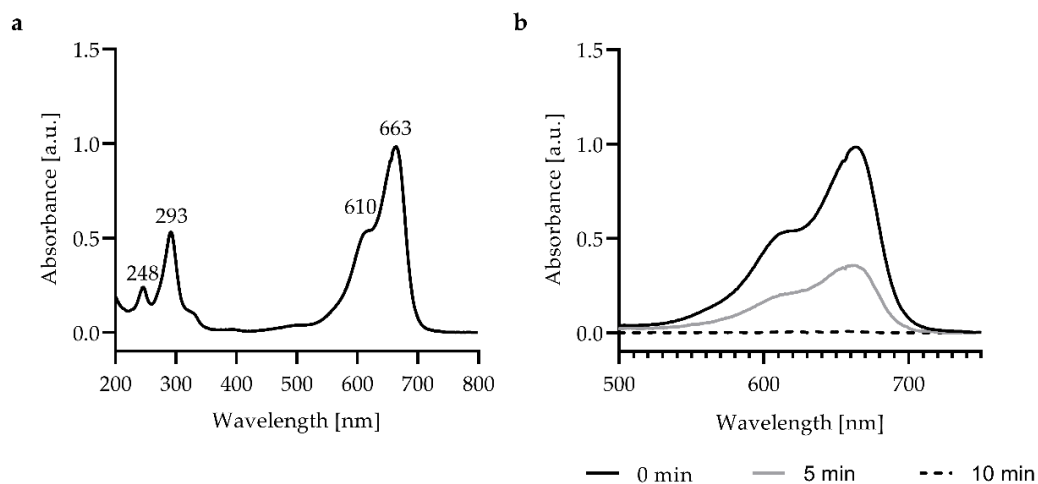


Figure 4. (a) UV–Vis spectrum of MB. (b) Reduction in the characteristic MB peak at 663 nm due to the photocatalytic activity of TiO₂.

The UV–Vis spectrum of pure MB (Figure 4a) showed a main absorption peak in the visible light region with a maximum at 663 nm and a small shoulder at 610 nm [48]. According to Pahang et al., the 663 nm peak might be attributable to the resonance of the π electrons of sulfur that resonate with those of the C electrons in the thiazinic center, and the peak at 610 nm corresponds to the π – π^* transition of benzene rings [49]. Other studies have explained the two absorption peaks as follows: the absorption peak at 663 nm is related to a MB monomer, which is the conjugation system between the two dimethylamine-substituted aromatic rings through sulfur and nitrogen atoms [50,51], and the shoulder peak at about 613 nm is attributed to the MB dimer [50,52]. With these peaks being responsible for the blue coloration of an aqueous MB solution [53], the degradation of MB by the photocatalytic TiO₂ was investigated in this wavelength range (Figure 4b). Furthermore, two absorption peaks were present in the UV region at 248 nm and 293 nm associated with substituted benzene rings [50,51,54]. The recorded UV–Vis spectrum of MB is in line with other studies [55–57].

After UV irradiation at 50 W/m² for 10 min and subsequent centrifugation of the solution to remove the TiO₂ particles, a colorless liquid was observed. This could be also detected in the UV–Vis spectrum: the addition of TiO₂ to the MB solution and the UV irradiation resulted in a decrease in the absorption peak at 610 nm and 663 nm, which is also consistent with other studies [58,59]. With increasing irradiation time, the absorption in this wavelength range decreased close to 0 a.u., which could explain the colorless appearance of the solution. The decrease in the absorption peaks could be due to the photocatalytic degradation of MB to leuco-MB [60]. Therefore, the successful degradation of MB by AEROXIDE® TiO₂ P25 irradiation was assumed.

Figure 5 shows the percentages of MB in the solutions of unirradiated and 48 h UV-irradiated specimens. The MB solution decolorized during the course of the test until it turned into a transparent liquid. The discoloration was increased in samples containing TiO₂. It should be noted that the optical density of the pure MB solution was set to 100% for each measuring point and the values of the test samples were normalized to this (Equation (1)). Differences in the percentage of MB in the solution among all samples were tested for statistical significance only at the 150 min time point.

The percentage of MB in the solution decreased from 100% (initial value) to $43 \pm 14\%$ over the course of 150 min for MF_0. The MF_0 specimen (48 h) behaved similarly, resulting in an MB concentration of $38 \pm 18\%$ after 150 min. Samples including TiO₂ showed a statistically significantly higher MB degradation than either MF_0 or MF_0 (48 h) after 150 min of UV irradiation ($p < 0.0001$). However, no statistically significant difference was observed in the degradation behavior of MB among the samples with different wt% TiO₂ values. When comparing unirradiated and 48 h UV-irradiated specimens with the same TiO₂ content, a statistically significantly increased MB degradation was observed after 150 min ($p < 0.01$ for MF_5 (48 h); $p < 0.05$ for MF_10 (48 h), MF_15 (48 h), and MF_20 (48 h)).

The decrease in MB for non-additivated samples might be because the degree of MB discoloration depends on experimental conditions such as pH and temperature [61]. UV irradiation of MF can result in the release of ammonia, causing the pH value to change and accelerating the MB degradation [62]. Furthermore, photobleaching (discoloration by irradiation) of MB is also possible [63], although Ramli et al. showed that photobleaching of MB is considerably weaker than degradation by UV-irradiated TiO₂ [64].

Despite the disadvantages of this method outlined above, clear trends were detected in the discoloration of MB. Unlike the pure MF, the additivated samples displayed an acceleration in the degradation of MB, which could be attributable to the formation of ROS. After 150 min, the average MB content was 12% or lower. The decrease in MB was even greater for the 48 h UV-irradiated samples. This could mean that the amount of TiO₂ particles accessible on the surface of the samples increased as a result of the irradiation, in turn increasing the photocatalytic activity [34].

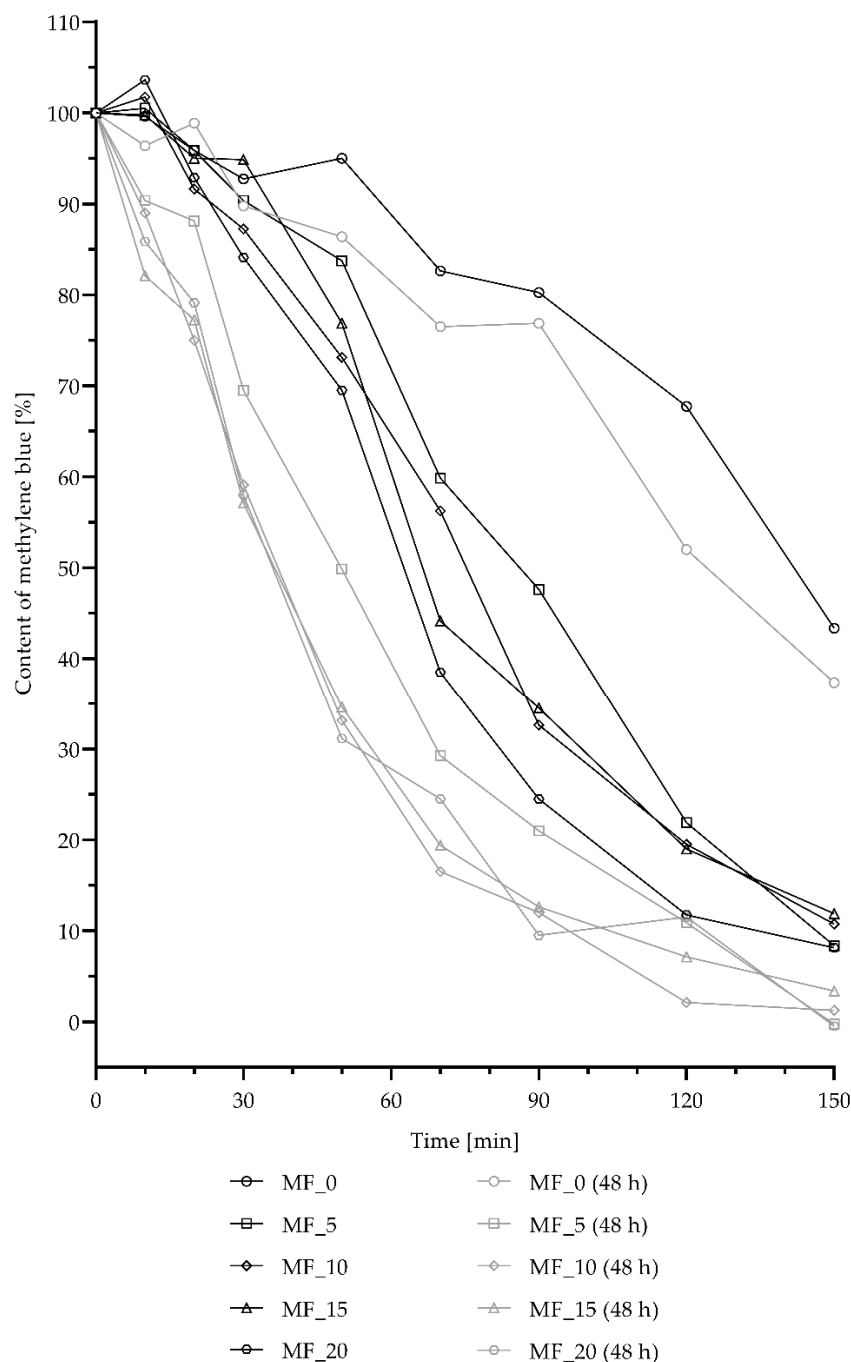


Figure 5. Degradation of MB. A distinction is made between samples tested directly and those irradiated beforehand for 48 h with UV light ($n = 3$).

2.5. Antimicrobial Activity

Antimicrobial tests were performed on MF_0, MF_10, MF_20, MF_0 (48 h), MF_10 (48 h), and MF_20 (48 h). The samples were irradiated for 2 h through both a UV-permeable and a UV-impermeable film. The results of the tests are shown in Figure 6.

For both types of film, none of the specimens MF_0, MF_10, and MF_20 showed any decrease in colony-forming units (CFUs) beyond one logarithm level.

Carré et al. demonstrated that AEROXIDE® TiO₂ P25 added to water successfully inactivated *Escherichia coli* (*E. coli*) when irradiated with UV light [65]. Therefore, we assume that the AEROXIDE® TiO₂ P25 incorporated in MF could not be photocatalytically activated, which is why no reduction in CFUs was observed for samples MF_10 and MF_20.

This could be due to the aforementioned polymer layer shielding the TiO₂ nanoparticles from UV light, as well as to water and oxygen, which inhibit the photocatalytic effect and, in turn, the antimicrobial effect [34].

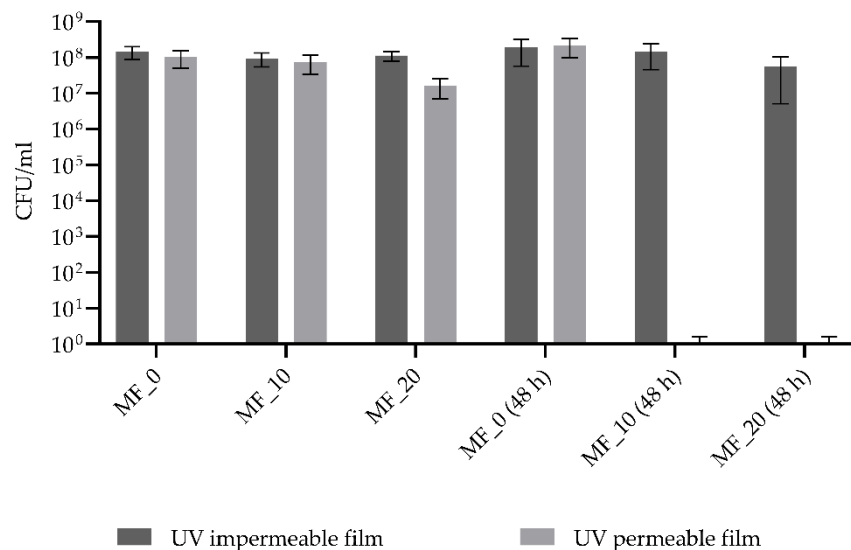


Figure 6. Antimicrobial surface activity of the modified MF against *E. coli*. The dark gray bars represent the CFUs of the samples covered with a UV-impermeable film, and the light gray bars represent those samples covered with a UV-permeable film. In addition, a distinction is made between specimens that have not been irradiated with UV light (MF_0, MF_10, and MF_20) and specimens irradiated for 48 h (MF_0 (48 h), MF_10 (48 h), and MF_20 (48 h)). ($n = 3, i = 2$).

Díez-Pascual et al. showed that polyphenylsulfone incorporating up to 5 wt% TiO₂ exhibited antimicrobial activity against *E. coli* and *Staphylococcus aureus* (*S. aureus*), even without any UV irradiation. *E. coli* was reduced by about 2.25 logarithm levels and *S. aureus* was reduced by 1.3 logarithm levels. Moreover, the antimicrobial effect was increased even further by UV irradiation [66]. Unlike our study, a TiO₂ powder consisting of 99.8% anatase was used here [66]. The observation that TiO₂, particularly the anatase phase, is toxic even in the absence of irradiation, has also been reported in other studies [67,68]. However, the exact mode of action is not fully understood, and various explanations have been reported [66,67,69–71]: the adsorption of the nanoparticles on the surface of the organism can lead to physicochemical interactions between TiO₂ and the organism, resulting in alteration of bacterial biomolecules and damage to the cells; redox reactions at the interface between the organism and nanoparticles can lead to oxidative degradation of the cell membrane; the uptake of nanoparticles into the cell can result in DNA damage.

The specimens MF_10 (48 h) and MF_20 (48 h) covered with a UV-permeable film showed a total CFU reduction after 2 h of UV irradiation, whereas MF_0 (48 h) and samples covered with a UV-impermeable film showed no reduction. Therefore, it was concluded that the antimicrobial effect against *E. coli* had to be due to the photocatalytically active TiO₂, although no difference was observed between 10 and 20 wt% TiO₂ after 2 h of UV irradiation.

The effective inactivation of *E. coli* by photocatalytically active TiO₂ was also demonstrated in other studies. Pal et al. showed that the inactivation rate of bacteria was enhanced by increasing irradiation duration and TiO₂ content and that *E. coli*, in particular, was inactivated by the photocatalytic effect [72]. Therefore, a shorter UV irradiation time could be assumed for MF_20 (48 h) compared to MF_10 (48 h) to achieve the same CFU reduction. Furthermore, a previous UV irradiation of the samples seems to be a prerequisite for obtaining an antimicrobial effect. The photocatalytic antimicrobial effect of TiO₂ appears to be greater against Gram-negative bacteria such as *E. coli* than Gram-positive bacteria [73], so

testing of the effect of MF_10 (48 h) and MF_20 (48 h) should be conducted and confirmed with further germs.

In addition, lower TiO₂ concentrations and UV stabilities of the samples should be investigated in more detail and additives should be used to increase long-term stability.

3. Materials and Methods

The samples were obtained by incorporation of AEROXIDE[®] TiO₂ P25 (Evonik Industries AG, Essen, Germany) into the thermoset MELOPAS[®] MF 152.7 (Raschig GmbH, Ludwigshafen am Rhein, Germany).

AEROXIDE[®] TiO₂ P25 is supplied by the manufacturer as a powder composed of anatase (76.3 ± 1.5 wt%), rutile (10.6 ± 0.3 wt%), and a proportion of amorphous TiO₂ (13.0 wt%) [35]. Ohtani et al. found a similar P25 composition comprising anatase (78%), rutile (14%), and amorphous (8%) [74]. According to Tobaldi et al., the average crystalline domain size of anatase is 15.5 ± 0.3 nm and that of rutile is 19.3 ± 0.6 nm [35]. The TiO₂ particles have a specific surface area of 50 ± 15 m²/g [65,75]. Previously published studies assigned a band gap energy of about 3.02 to 3.20 eV to the P25 [75–78] and determined 365 nm as an appropriate wavelength for activating the photocatalytic effect [65,79,80]. A similar UV source was, therefore, also selected for this study.

MELOPAS[®] MF 152.7 is a cellulose-reinforced melamine molding compound and is supplied by the manufacturer in granulate form. It is characterized by its good electrical properties and high surface hardness, as well as its resistance to abrasion, UV, and chemical impacts. The polymer is a light-colored material used for insulation and installation purposes and is resistant to leakage current and high temperatures. It is also found in fittings for household appliances as well as in tableware for eating and drinking [28]. Figure 7 gives a brief overview of the methods used in this study and the test procedure. Test specimens were produced to determine their mechanical and chemical properties and to evaluate their long-term stabilities and antimicrobial properties.

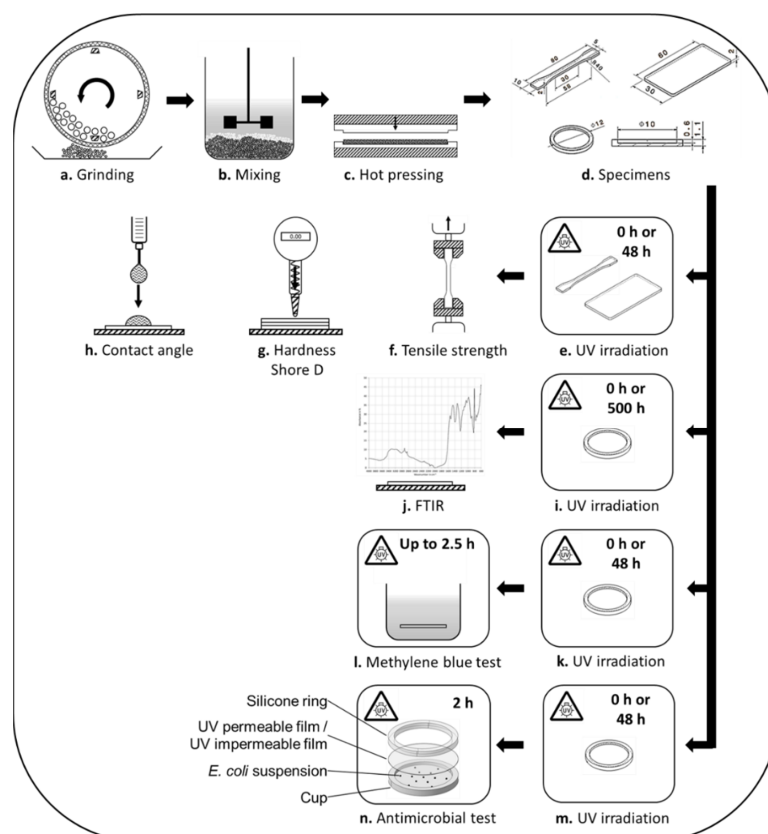


Figure 7. Overview of the used methods and flow of the experiment.

All results are presented as mean and standard deviation values. In the descriptions of Figures 1, 2, 5 and 6, “*n*” indicates the number of specimens examined and “*i*” indicates the number of measurements performed per specimen.

3.1. Production and Preparation of Test Specimens

In order to achieve a good dispersion of the TiO₂ powder within the thermoset, the polymer granulate was first ground in a mill at 7000 rpm (Pulverisette 14, FRITSCH GmbH, Idar-Oberstein, Germany). One hundred milliliters of ethanol was then added to 100 g of the ground polymer and the mixture stirred to create a homogenous suspension. TiO₂ powder was added at different weight percentages (5, 10, 15, and 20 wt% TiO₂) and, again, 50 mL of ethanol was added and the mixture stirred. The mixture was then kept in an ultrasonic bath (Sonorex SUPER RK 255H, BANDELIN electronic GmbH & Co. KG, Berlin, Germany) for 60 min to increase dispersion. Thereafter, the mixture was stored in a laboratory hood to expel the solvent before being processed into samples using a hot press (300P, Dr. Collin GmbH, Ebersberg, Germany) for 2 min at 250 bar and 185 °C. Three specimen geometries were produced for the individual tests; these are presented later. A dog-bone type 1 BA was produced for determining the tensile strength according to DIN EN ISO 527-2:2012-06, along with a plate for determining the Shore D hardness according to EN ISO 868:2003-10 and the dispersion of the TiO₂. The cups required for microbiological testing and photocatalytic activity testing were also produced

All tests were performed on samples that had not been exposed to UV irradiation, as well as on samples that had been exposed to UV light for 48 h in a weathering chamber (Q-Sun Xe-1, Q-Lab, Westlake, OH, USA).

To evaluate the long-term chemical stability, samples irradiated with UV light in a weathering chamber for 500 h were also included. The UV range of the sunlight spectrum was simulated by a xenon arc lamp with a UV light intensity of 50 W/m².

For simplicity, the sample designations listed in Table 1 are used in this paper. Specimens irradiated with UV light for 48 or 500 h are indicated in diagrams by the suffix (48 h) or (500 h).

Table 1. Sample designations and compositions.

Abbreviation	Content	Content
	MELOPAS [®] MF 152.7 (wt%)	AEROXIDE [®] TiO ₂ P25 (wt%)
MF_0	100	0
MF_5	95	5
MF_10	90	10
MF_15	85	15
MF_20	80	20

3.2. Mechanical Tests

To determine the influence of the additive concentration, the mechanical properties of the test specimens were determined and compared with the manufacturer’s specifications [23]. The tensile strength of the specimens was determined according to DIN EN ISO 527-2:2012-06 and the hardness according to EN ISO 868:2003-10.

To determine the effect of the amount of TiO₂ and the activated photocatalytic effect on the material, tensile strength was investigated for both unirradiated specimens and specimens irradiated for 48 h. Eight unirradiated and eight irradiated dog-bones of the different TiO₂ contents (0 to 20 wt%) were tested, 0 wt% TiO₂ serving as a control. A tensile strength machine (Z 2,5 SN153778 DN491473, ZwickRoell GmbH & Co. KG, Ulm, Germany) was used for this purpose. A preload of 0.05 N/mm², a traverse acceleration of 20 mm/min, and a predefined initial length of 58 mm were selected as parameters. A PCE-DDA 10-ICA hardness tester (PCE Deutschland GmbH Prüfgeräte, Meschede, Germany) was used to determine the Shore D hardness for unirradiated and irradiated (48 h) specimens at five different points on each sample to create a total of 15 measured values per sample.

3.3. Contact Angle Measurement

The contact angle of water was measured on samples that were not exposed and samples that were exposed to UV irradiation (48 h) using a DSA25E apparatus (Krüss GmbH, Hamburg, Germany). Three test specimens were measured per TiO₂ content. Distilled water was used as the test liquid, of which five drops were measured per specimen.

3.4. FTIR Spectroscopy

Samples containing 0, 10, and 20 wt% TiO₂ were irradiated with UV light for 0 and 500 h and analyzed by FTIR spectroscopy (FTIR VERTEX 70, Bruker Optik GmbH, Ettlingen, Germany) using an ATR unit and a wavenumber range of 600 to 4000 cm⁻¹.

3.5. Methylene Blue Test

The degradation of MB in the presence of TiO₂ can be used to derive information about the photocatalytic activity of TiO₂ [62,81]. Both unirradiated specimens and specimens irradiated for 48 h were analyzed. The generated radicals resulted in a transformation from a blue dye (MB) to a colorless liquid (leuco-MB) [60]. The trial was performed in accordance with DIN 52980:2008-10. The specimens (cups) were placed in a well plate and wetted with 2 mL of an MB solution (20 µmol/L). The prepared samples were irradiated in the weathering chamber at a light intensity of 50 W/m² for 150 min. The optical density of the liquid was initially measured every 10 min, after 30 min every 20 min, and after 90 min every 30 min. The optical density was determined by a Multiskan™ FC Microplate Photometer (Thermo Fisher Scientific, Waltham, MA, USA) at a wavelength of 620 nm, corresponding to the absorption peak of MB [47,82,83]. In the evaluation, the percentage of MB in % of each material sample was determined. Equation (1) was used for this purpose, with MB representing the MB content in %, OD_t the optical density at the time t, OD_W the optical density of water, and OD_R the optical density of the reference sample at the time t.

$$MB = \frac{OD_t - OD_W}{OD_R - OD_W} * 100\% \quad (1)$$

The evaluation of pure MB is necessary for observing the discoloration of the MB solution due to UV light over the test period.

In addition, UV-Vis spectra were recorded both for an MB solution and two degraded MB solutions. For this purpose, 0.01 g (LA230S, Sartorius AG, Göttingen, Germany) of TiO₂ powder was added to 5 mL of MB (20 µmol/L), which was then irradiated with UV light in the weathering chamber at an intensity of 50 W/m² for 5 and 10 min. After irradiation, the solution was centrifuged (Universal 320, Andreas Hettich GmbH & Co. KG, Tuttlingen, Germany) three times at 4000 rpm for 40 min to remove the TiO₂ particles. The spectra of the solutions were recorded over a wavelength range of 200 to 800 nm using an AvaLight-D(H)-S light source and AvaSpec-ULS2048CL-EVO spectrometer (Avantes, Apeldoorn, The Netherlands).

3.6. Examination of the Antimicrobial Effect

In order to measure the antimicrobial surface effect of unirradiated specimens (MF_0, MF_10, and MF_20) and specimens irradiated for 48 h (MF_0 (48 h), MF_10 (48 h), and MF_20 (48 h)), the test cups were contaminated with an *E. coli* suspension. Ten microliters of the bacterial suspension were added to each sample. The bacterial suspension was cultured in dilution series (up to 10⁻⁷) on agar plates (LB-Miller-Agar) to determine the original bacterial concentration. To prevent the bacteria suspension from drying out, UV-permeable films were applied to the cups, which were then weighed down with a silicone ring to create a seal. UV-impermeable films were placed alongside the UV-permeable films on appropriate reference samples to ensure that the control samples were exposed to the same conditions as the test samples but were not irradiated. The samples were then irradiated in a specially developed UV chamber (λ = 365 nm, 4 to 5 W/m²) for 2 h.

After irradiation, the specimens were placed in 1 mL of phosphate-buffered saline (PBS) with 0.1 vol. % polysorbate 80 (Tween) and vortexed for 2 min to dissolve the bacteria from the samples (to increase this effect, it is possible to add sterile glass beads to the PBS). After completing this step, dilution series (up to 10^{-7}) were produced from the PBS, and 100 μ L was plated onto LB-Miller agar. The bacteria were incubated at 37 °C for 24 h. After incubation, the CFUs were counted, and the antimicrobial effect of the samples was determined in relation to the reference.

3.7. Statistical Analysis

A statistical evaluation was performed of the mechanical properties (tensile strength and hardness Shore D), contact angles, and MB degradation.

The effect of TiO₂ content on mechanical properties and contact angle was verified by a one-way ANOVA ($\alpha = 0.05$). The effect of UV irradiation was verified with an unpaired Student's t-test ($\alpha = 0.05$).

The effect of TiO₂ content on MB degradation was verified after 150 min of UV irradiation with a one-way ANOVA ($\alpha = 0.05$). The effect of UV irradiation was verified with an unpaired Student's t-test ($\alpha = 0.05$).

The normal distribution was verified using a Kolmogorov–Smirnov test ($\alpha = 0.05$).

A *p*-value of <0.05 was considered significant. The statistical analyses were performed with GraphPad Prism 9 (version number 9.4.0 (673), GraphPad Software, San Diego, CA, USA) and MS Excel 2019 (version number 1808, Microsoft Corporation, Redmond, WA, USA).

4. Conclusions

Photocatalytically active samples were successfully produced using the MELOPAS[®] MF 152.7 thermoset and the AEROXIDE[®] TiO₂ P25 additive. Compounds were produced with up to 20 wt% TiO₂. A decrease in tensile strength was observed with increasing additive content, and the Shore D hardness changed significantly for MF_5 and MF_10. However, even though the tensile strength of the compounds was altered by the additive content, it remained above or within the range of the manufacturer's specifications for MF. The incorporation of TiO₂ in the thermosets produced no change in the chemical structure of MF.

Irradiation of the additivated samples with UV light demonstrated the photocatalytic effect of TiO₂ by reducing the contact angle and degrading MB. During 150 min, an MB degradation of up to 88% was observed for the additivated samples. A previous irradiation for 48 h accelerated the degradation even further and a complete MB degradation could be achieved after 150 min of UV irradiation. The MB degradation confirmed the photocatalytic activity of the fabricated MF-TiO₂ compound. Furthermore, a decrease in tensile strength due to UV irradiation was measured, whereas no effect on Shore D hardness was detected. However, a 500 h irradiation with UV light led to a change in the chemical spectrum, suggesting aging of MF.

For the test specimens MF_10 and MF_20, no antimicrobial effect of more than one logarithm level was measured. However, if the samples were irradiated with UV light for 48 h before the antimicrobial tests were carried out, a complete reduction in *E. coli* was achieved after de novo UV irradiation for 2 h. UV irradiation for a period of 48 h must, therefore, be regarded as a necessary pretreatment for creating an antimicrobial effect.

Overall, an antimicrobial thermoset was successfully produced by incorporating photocatalytically active TiO₂ nanoparticles into the MF. In medical facilities, the developed compound could find application as a means of reducing the spread of pathogens.

Author Contributions: Conceptualization, T.F.; methodology, M.A. and T.F.; investigation, N.Z. and M.A.; resources, M.A., S.Y. and T.F.; writing—original draft preparation, M.A. and P.M.; writing—review and editing, M.A., N.Z., S.Y., M.E. and P.M.; visualization, M.A.; supervision, M.E. and P.M.; funding acquisition, S.Y., T.H., M.B. and M.E. All authors have read and agreed to the published version of the manuscript.

Funding: This IGF Project 19079 N of the FSKZ e.V. research association was funded via Arbeitsgemeinschaft industrieller Forschungsvereinigungen “Otto von Guericke” e.V. (AiF) within the program for promoting the Industrial Collective Research (IGF) of the German Ministry of Economic Affairs and Energy (BMWi), based on a resolution of the German Parliament.

Data Availability Statement: Data can be provided upon request.

Acknowledgments: The authors would like to express their gratitude to Evonik Industries AG and Raschig GmbH for supporting this research with their material. Furthermore, the authors would like to thank the library of the Technical University of Munich for supporting the publication process.

Conflicts of Interest: The authors declare that they have no conflict of interest. The funders had no role in the design of the study; in the collection, analyses, or interpretation of data; in the writing of the manuscript; or in the decision to publish the results.

References

1. Breathnach, A.S. Nosocomial Infections and Infection Control. *Medicine* **2013**, *41*, 649–653. [[CrossRef](#)]
2. Ott, E.; Saathoff, S.; Graf, K.; Schwab, F.; Chaberny, I.F. The Prevalence of Nosocomial and Community Acquired Infections in a University Hospital. *Dtsch. Arztebl. Int.* **2013**, *110*, 533–540. [[CrossRef](#)] [[PubMed](#)]
3. Page, K.; Wilson, M.; Parkin, I.P. Antimicrobial Surfaces and Their Potential in Reducing the Role of the Inanimate Environment in the Incidence of Hospital-Acquired Infections. *J. Mater. Chem.* **2009**, *19*, 3819–3831. [[CrossRef](#)]
4. Khan, H.A.; Baig, F.K.; Mehboob, R. Nosocomial Infections: Epidemiology, Prevention, Control and Surveillance. *Asian Pac. J. Trop. Biomed.* **2017**, *7*, 478–482. [[CrossRef](#)]
5. Weber, D.J.; Rutala, W.A. Self-Disinfecting Surfaces: Review of Current Methodologies and Future Prospects. *Am. J. Infect. Control* **2013**, *41*, 31–35. [[CrossRef](#)] [[PubMed](#)]
6. Humphreys, H. Self-Disinfecting and Microbiocide-Impregnated Surfaces and Fabrics: What Potential in Interrupting the Spread of Healthcare-Associated Infection? *Clin. Infect. Dis.* **2013**, *58*, 848–853. [[CrossRef](#)]
7. Radheshkumar, C.; Münstedt, H. Antimicrobial Polymers from Polypropylene/Silver Composites—Ag⁺ Release Measured by Anode Stripping Voltammetry. *React. Funct. Polym.* **2006**, *66*, 780–788. [[CrossRef](#)]
8. Thokala, N.; Kealey, C.; Kennedy, J.; Brady, D.B.; Farrell, J.B. Characterisation of Polyamide 11/Copper Antimicrobial Composites for Medical Device Applications. *Mater. Sci. Eng. C* **2017**, *78*, 1179–1186. [[CrossRef](#)]
9. Park, G.W.; Cho, M.; Cates, E.L.; Lee, D.; Oh, B.-T.; Vinjé, J.; Kim, J.-H. Fluorinated TiO₂ as an Ambient Light-Activated Virucidal Surface Coating Material for the Control of Human Norovirus. *J. Photochem. Photobiol. B Biol.* **2014**, *140*, 315–320. [[CrossRef](#)]
10. Bogdan, J.; Zarzyńska, J.; Pławińska-Czarnak, J. Comparison of Infectious Agents Susceptibility to Photocatalytic Effects of Nanosized Titanium and Zinc Oxides: A Practical Approach. *Nanoscale Res. Lett.* **2015**, *10*, 309. [[CrossRef](#)]
11. De Jong, B.; Meeder, A.M.; Koekkoek, K.W.A.C.; Schouten, M.A.; Westers, P.; van Zanten, A.R.H. Pre-Post Evaluation of Effects of a Titanium Dioxide Coating on Environmental Contamination of an Intensive Care Unit: The TITANIC Study. *J. Hosp. Infect.* **2018**, *99*, 256–262. [[CrossRef](#)] [[PubMed](#)]
12. Wang, S.; Song, Y.; Jiang, L. Photoresponsive Surfaces with Controllable Wettability. *J. Photochem. Photobiol. C Photochem. Rev.* **2007**, *8*, 18–29. [[CrossRef](#)]
13. Foster, H.A.; Ditta, I.B.; Varghese, S.; Steele, A. Photocatalytic Disinfection Using Titanium Dioxide: Spectrum and Mechanism of Antimicrobial Activity. *Appl. Microbiol. Biotechnol.* **2011**, *90*, 1847–1868. [[CrossRef](#)] [[PubMed](#)]
14. De Pasquale, I.; Lo Porto, C.; Dell’Edera, M.; Petronella, F.; Agostiano, A.; Curri, M.L.; Comparelli, R. Photocatalytic TiO₂-Based Nanostructured Materials for Microbial Inactivation. *Catalysts* **2020**, *10*, 1382. [[CrossRef](#)]
15. Prakash, J.; Cho, J.; Mishra, Y.K. Photocatalytic TiO₂ Nanomaterials as Potential Antimicrobial and Antiviral Agents: Scope Against Blocking the SARS-CoV-2 Spread. *Micro Nano Eng.* **2022**, *14*, 100100. [[CrossRef](#)]
16. Micochova, P.; Chadha, A.; Hesseloj, T.; Fraternali, F.; Ramsden, J.J.; Gupta, R.K. Rapid Inactivation of SARS-CoV-2 by Titanium Dioxide Surface Coating. *Wellcome Open Res.* **2021**, *6*, 56. [[CrossRef](#)]
17. Khaiboullina, S.; Uppal, T.; Dhabarde, N.; Subramanian, V.R.; Verma, S.C. Inactivation of Human Coronavirus by Titania Nanoparticle Coatings and UVC Radiation: Throwing Light on SARS-CoV-2. *Viruses* **2021**, *13*, 19. [[CrossRef](#)]
18. Hamza, R.Z.; Gobouri, A.A.; Al-Yasi, H.M.; Al-Talhi, T.A.; El-Megharbel, S.M. A New Sterilization Strategy Using TiO₂ Nanotubes for Production of Free Radicals that Eliminate Viruses and Application of a Treatment Strategy to Combat Infections Caused by Emerging SARS-CoV-2 during the COVID-19 Pandemic. *Coatings* **2021**, *11*, 680. [[CrossRef](#)]
19. Hashimoto, K.; Irie, H.; Fujishima, A. TiO₂ Photocatalysis: A Historical Overview and Future Prospects. *Jpn. J. Appl. Phys.* **2005**, *44*, 8269–8285. [[CrossRef](#)]
20. Wang, C.; Cao, S.; Tie, X.; Qiu, B.; Wu, A.; Zheng, Z. Induction of Cytotoxicity by Photoexcitation of TiO₂ Can Prolong Survival in Glioma-Bearing Mice. *Mol. Biol. Rep.* **2010**, *38*, 523–530. [[CrossRef](#)]
21. Parham, S.; Wicaksono, D.H.B.; Bagherbaigi, S.; Lee, S.L.; Nur, H. Antimicrobial Treatment of Different Metal Oxide Nanoparticles: A Critical Review. *J. Chin. Chem. Soc.* **2016**, *63*, 385–393. [[CrossRef](#)]

22. Ali, S.S.; Qazi, I.A.; Arshad, M.; Khan, Z.; Voice, T.C.; Mehmood, C.T. Photocatalytic Degradation of Low Density Polyethylene (LDPE) Films Using Titania Nanotubes. *Environ. Nanotechnol. Monit. Manag.* **2016**, *5*, 44–53. [[CrossRef](#)]
23. Zhao, X.U.; Li, Z.; Chen, Y.; Shi, L.; Zhu, Y. Solid-Phase Photocatalytic Degradation of Polyethylene Plastic under UV and Solar Light Irradiation. *J. Mol. Catal. A Chem.* **2007**, *268*, 101–106. [[CrossRef](#)]
24. Shang, J.; Chai, M.; Zhu, Y. Solid-Phase Photocatalytic Degradation of Polystyrene Plastic with TiO₂ as Photocatalyst. *J. Solid State Chem.* **2003**, *174*, 104–110. [[CrossRef](#)]
25. Soitong, T.; Wongsanmai, S. Photo-Oxidative Degradation Polyethylene Containing Titanium Dioxide and Poly(Ethylene Oxide). *Key Eng. Mater.* **2017**, *751*, 796–800. [[CrossRef](#)]
26. Kim, S.H.; Kwak, S.-Y.; Suzuki, T. Photocatalytic Degradation of Flexible PVC/TiO₂ Nanohybrid as an Eco-Friendly Alternative to the Current Waste Landfill and Dioxin-Emitting Incineration of Post-Use PVC. *Polymer* **2006**, *47*, 3005–3016. [[CrossRef](#)]
27. Bhushan, B.; Gupta, B.K. *Handbook of Tribology: Materials, Coatings, and Surface Treatments*; McGraw-Hill: New York, NY, USA, 1991.
28. Fotovvati, B.; Namdari, N.; Dehghanghadikolaei, A. On Coating Techniques for Surface Protection: A Review. *J. Manuf. Mater. Process* **2019**, *3*, 28. [[CrossRef](#)]
29. Francolini, I.; Vuotto, C.; Piozzi, A.; Donelli, G. Antifouling and Antimicrobial Biomaterials: An Overview. *Apmis* **2017**, *125*, 392–417. [[CrossRef](#)]
30. Cloutier, M.; Mantovani, D.; Rosei, F. Antibacterial Coatings: Challenges, Perspectives, and Opportunities. *Trends Biotechnol.* **2015**, *33*, 637–652. [[CrossRef](#)]
31. Fischer, T.; Suttor, S.; Mansi, S.; Osthues, L.; Mela, P. Antimicrobial Silicone Rubbers Based on Photocatalytically Active Additives. *J. Appl. Polym. Sci.* **2021**, *138*, 51352. [[CrossRef](#)]
32. Raschig GmbH. *Material Safety Data Sheet MELOPAS[®] MF 152.7*; Raschig GmbH: Ludwigshafen am Rhein, Germany, 2014.
33. Carballeira, P.; Hauptert, F. Toughening Effects of Titanium Dioxide Nanoparticles on TiO₂/Epoxy Resin Nanocomposites. *Polym. Compos.* **2010**, *31*, 1241–1246. [[CrossRef](#)]
34. Man, C.; Zhang, C.; Liu, Y.; Wang, W.; Ren, W.; Jiang, L.; Reisdorffer, F.; Nguyen, T.P.; Dan, Y. Poly (Lactic Acid)/Titanium Dioxide Composites: Preparation and Performance under Ultraviolet Irradiation. *Polym. Degrad. Stab.* **2012**, *97*, 856–862. [[CrossRef](#)]
35. Tobaldi, D.M.; Pullar, R.C.; Seabra, M.P.; Labrincha, J.A. Fully Quantitative X-ray Characterisation of Evonik Aeroxide TiO₂ P25[®]. *Mater. Lett.* **2014**, *122*, 345–347. [[CrossRef](#)]
36. Asiaban, S.; Taghinejad, S.F. Investigation of the Effect of Titanium Dioxide on Optical Aspects and Physical and Mechanical Characteristics of ABS Polymer. *J. Elastomers Plast.* **2010**, *42*, 267–274. [[CrossRef](#)]
37. Sakai, N.; Fujishima, A.; Watanabe, T.; Hashimoto, K. Quantitative Evaluation of the Photoinduced Hydrophilic Conversion Properties of TiO₂ Thin Film Surfaces by the Reciprocal of Contact Angle. *J. Phys. Chem. B* **2003**, *107*, 1028–1035. [[CrossRef](#)]
38. Völz, H.G.; Kaempf, G.; Fitzky, H.G.; Klaeren, A. The Chemical Nature of Chalking in the Presence of Titanium Dioxide Pigments. In *Photodegradation and Photostabilization of Coatings*; ACS Symposium Series; American Chemical Society: Washington, DC, USA, 1981; Volume 151, pp. 163–182.
39. Allen, N.S.; Edge, M.; Ortega, A.; Sandoval, G.; Liauw, C.M.; Verran, J.; Stratton, J.; McIntyre, R.B. Degradation and Stabilisation of Polymers and Coatings: Nano versus Pigmentary Titania Particles. *Polym. Degrad. Stab.* **2004**, *85*, 927–946. [[CrossRef](#)]
40. Rezaei, R.; Khalifeh, R.; Rajabzadeh, M.; Dorosty, L.; Doroodmand, M.M. Melamine-Formaldehyde Resin Supported H⁺-Catalyzed Three-Component Synthesis of 1,8-Dioxo-Decahydroacridine Derivatives in Water and under Solvent-Free Conditions. *Heterocycl. Commun.* **2013**, *19*, 57–63. [[CrossRef](#)]
41. Merline, D.J.; Vukusic, S.; Abdala, A.A. Melamine Formaldehyde: Curing Studies and Reaction Mechanism. *Polym. J.* **2013**, *45*, 413–419. [[CrossRef](#)]
42. Jiang, Z.; Liu, G. Microencapsulation of Ammonium Polyphosphate with Melamine-Formaldehyde-Tris(2-hydroxyethyl)Isocyanurate Resin and its Flame Retardancy in Polypropylene. *RSC Adv.* **2015**, *5*, 88445–88455. [[CrossRef](#)]
43. Sriwong, C.; Choojun, K.; Sriwong, S. High Photocatalytic Performance of 3D Porous-Structured TiO₂@Natural Rubber Hybrid Sheet on the Removal of Indigo Carmine Dye in Water. *SN Appl. Sci.* **2019**, *1*, 864. [[CrossRef](#)]
44. Liu, Z.; Jian, Z.; Fang, J.; Xu, X.; Zhu, X.; Wu, S. Low-Temperature Reverse Microemulsion Synthesis, Characterization, and Photocatalytic Performance of Nanocrystalline Titanium Dioxide. *Int. J. Photoenergy* **2012**, *2012*, 702503. [[CrossRef](#)]
45. Kim, H.S.; Lee, Y.J.; Koo, Y.J.; Pack, E.C.; Lim, K.M.; Choi, D.W. Migration of Monomers, Plastic Additives, and Non-Intentionally Added Substances from Food Utensils Made of Melamine-Formaldehyde Resin Following Ultraviolet Sterilization. *Food Control* **2021**, *125*, 107981. [[CrossRef](#)]
46. Doi, T.; Yamamoto, T. Optical Etching to Pattern Microstructures on Plastics by Vacuum Ultraviolet Light. *Materials* **2020**, *13*, 2206. [[CrossRef](#)] [[PubMed](#)]
47. Houas, A.; Lachheb, H.; Ksibi, M.; Elaloui, E.; Guillard, C.; Herrmann, J.-M. Photocatalytic Degradation Pathway of Methylene Blue in Water. *Appl. Catal. B Environ.* **2001**, *31*, 145–157. [[CrossRef](#)]
48. Yang, C.; Dong, W.; Cui, G.; Zhao, Y.; Shi, X.; Xia, X.; Tang, B.; Wang, W. Highly Efficient Photocatalytic Degradation of Methylene Blue by P2ABSA-Modified TiO₂ Nanocomposite Due to the Photosensitization Synergetic Effect of TiO₂ and P2ABSA. *RSC Adv.* **2017**, *7*, 23699–23708. [[CrossRef](#)]
49. Pahang, F.; Parvin, P.; Ghafoori-Fard, H.; Bavali, A.; Moafi, A. Fluorescence Properties of Methylene Blue Molecules Coupled with Metal Oxide Nanoparticles. *OSA Contin.* **2020**, *3*, 688–697. [[CrossRef](#)]

50. Mondal, S.; De Anda Reyes, M.E.; Pal, U. Plasmon Induced Enhanced Photocatalytic Activity of Gold Loaded Hydroxyapatite Nanoparticles for Methylene Blue Degradation under Visible Light. *RSC Adv.* **2017**, *7*, 8633–8645. [[CrossRef](#)]
51. Rauf, M.A.; Meetani, M.A.; Khaleel, A.; Ahmed, A. Photocatalytic Degradation of Methylene Blue Using a Mixed Catalyst and Product Analysis by LC/MS. *Chem. Eng. J.* **2010**, *157*, 373–378. [[CrossRef](#)]
52. Flores, N.M.; Pal, U.; Galeazzi, R.; Sandoval, A. Effects of Morphology, Surface Area, and Defect Content on the Photocatalytic Dye Degradation Performance of ZnO Nanostructures. *RSC Adv.* **2014**, *4*, 41099–41110. [[CrossRef](#)]
53. Tardivo, J.P.; Del Giglio, A.; de Oliveira, C.S.; Gabrielli, D.S.; Junqueira, H.C.; Tada, D.B.; Severino, D.; de Fátima Turchiello, R.; Baptista, M.S. Methylene Blue in Photodynamic Therapy: From Basic Mechanisms to Clinical Applications. *Photodiagnosis Photodyn. Ther.* **2005**, *2*, 175–191. [[CrossRef](#)]
54. Khan, I.; Saeed, K.; Zekker, I.; Zhang, B.; Hendi, A.H.; Ahmad, A.; Ahmad, S.; Zada, N.; Ahmad, H.; Shah, L.A.; et al. Review on Methylene Blue: Its Properties, Uses, Toxicity and Photodegradation. *Water* **2022**, *14*, 242. [[CrossRef](#)]
55. Basu, M.; Sinha, A.K.; Pradhan, M.; Sarkar, S.; Pal, A.; Mondal, C.; Pal, T. Methylene Blue–Cu₂O Reaction Made Easy in Acidic Medium. *J. Phys. Chem. C* **2012**, *116*, 25741–25747. [[CrossRef](#)]
56. Melgoza, D.; Hernández-Ramírez, A.; Peralta-Hernández, J.M. Comparative Efficiencies of the Decolourisation of Methylene Blue Using Fenton's and Photo-Fenton's Reactions. *Photochem. Photobiol. Sci.* **2009**, *8*, 596–599. [[CrossRef](#)]
57. Dinh, V.-P.; Huynh, T.-D.-T.; Le, H.M.; Nguyen, V.-D.; Dao, V.-A.; Hung, N.Q.; Tuyen, L.A.; Lee, S.; Yi, J.; Nguyen, T.D.; et al. Insight into the Adsorption Mechanisms of Methylene Blue and Chromium(III) from Aqueous Solution onto Pomelo Fruit Peel. *RSC Adv.* **2019**, *9*, 25847–25860. [[CrossRef](#)]
58. Xu, J.; Zhang, T.; Zhang, J. Photocatalytic Degradation of Methylene Blue with Spent FCC Catalyst Loaded with Ferric Oxide and Titanium Dioxide. *Sci. Rep.* **2020**, *10*, 12730. [[CrossRef](#)]
59. Singh, N.; Jana, S.; Singh, G.P.; Dey, R.K. Graphene-Supported TiO₂: Study of Promotion of Charge Carrier in Photocatalytic Water Splitting and Methylene Blue Dye Degradation. *Adv. Compos. Hybrid Mater.* **2020**, *3*, 127–140. [[CrossRef](#)]
60. Kazemi, F.; Mohamadnia, Z.; Kaboudin, B.; Karimi, Z. Photodegradation of Methylene Blue with a Titanium Dioxide/Polyacrylamide Photocatalyst under Sunlight. *J. Appl. Polym. Sci.* **2016**, *133*, 43386. [[CrossRef](#)]
61. Rahim, S.; Sasani Ghamsari, M.; Radiman, S.; Hamzah, A. Highly Stable TiO₂ Sol with High Photocatalytic Properties. In *The Sol-Gel Process: Uniformity, Polymers and Applications*; Nova Science Publishers, Inc.: New York, NY, USA, 2011; pp. 773–785.
62. Salehi, M.; Hashemipour, H.; Mirzaee, M. Experimental Study of Influencing Factors and Kinetics in Catalytic Removal of Methylene Blue with TiO₂ Nanopowder. *Am. J. Environ. Eng.* **2012**, *2*, 1–7. [[CrossRef](#)]
63. Tang, J.; Zou, Z.; Yin, J.; Ye, J. Photocatalytic Degradation of Methylene Blue on CaIn₂O₄ under Visible Light Irradiation. *Chem. Phys. Lett.* **2003**, *382*, 175–179. [[CrossRef](#)]
64. Ramli, Z.A.C.; Asim, N.; Isahak, W.N.R.W.; Emdadi, Z.; Ahmad-Ludin, N.; Yarmo, M.A.; Sopian, K. Photocatalytic Degradation of Methylene Blue under UV Light Irradiation on Prepared Carbonaceous TiO₂. *Sci. World J.* **2014**, *2014*, 415136. [[CrossRef](#)]
65. Carré, G.; Hamon, E.; Ennahar, S.; Estner, M.; Lett, M.-C.; Horvatovich, P.; Gies, J.-P.; Keller, V.; Keller, N.; Andre, P. TiO₂ Photocatalysis Damages Lipids and Proteins in Escherichia coli. *Appl. Environ. Microbiol.* **2014**, *80*, 2573–2581. [[CrossRef](#)]
66. Díez-Pascual, A.M.; Díez-Vicente, A.L. Effect of TiO₂ Nanoparticles on the Performance of Polyphenylsulfone Biomaterial for Orthopaedic Implants. *J. Mater. Chem. B* **2014**, *2*, 7502–7514. [[CrossRef](#)]
67. Dalai, S.; Pakrashi, S.; Chakravarty, S.; Hussain, S.; Chandrasekaran, N.; Mukherjee, A. Studies on Interfacial Interactions of TiO₂ Nanoparticles with Bacterial Cells under Light and Dark Conditions. *Bull. Mater. Sci.* **2014**, *37*, 371–381. [[CrossRef](#)]
68. Li, W.; Zhang, C.; Chi, H.; Li, L.; Lan, T.; Han, P.; Chen, H.; Qin, Y. Development of Antimicrobial Packaging Film Made from Poly(Lactic Acid) Incorporating Titanium Dioxide and Silver Nanoparticles. *Molecules* **2017**, *22*, 1170. [[CrossRef](#)]
69. Sayes, C.M.; Wahi, R.; Kurian, P.A.; Liu, Y.; West, J.L.; Ausman, K.D.; Warheit, D.B.; Colvin, V.L. Correlating Nanoscale Titania Structure with Toxicity: A Cytotoxicity and Inflammatory Response Study with Human Dermal Fibroblasts and Human Lung Epithelial Cells. *Toxicol. Sci.* **2006**, *92*, 174–185. [[CrossRef](#)] [[PubMed](#)]
70. Adams, L.K.; Lyon, D.Y.; Alvarez, P.J.J. Comparative Eco-Toxicity of Nanoscale TiO₂, SiO₂, and ZnO Water Suspensions. *Water Res.* **2006**, *40*, 3527–3532. [[CrossRef](#)] [[PubMed](#)]
71. Kumar, A.; Pandey, A.K.; Singh, S.S.; Shanker, R.; Dhawan, A. Engineered ZnO and TiO₂ Nanoparticles Induce Oxidative Stress and DNA Damage Leading to Reduced Viability of Escherichia coli. *Free Radic. Biol. Med.* **2011**, *51*, 1872–1881. [[CrossRef](#)]
72. Pal, A.; Pehkonen, S.; Yu, L.; Ray, M. Photocatalytic Inactivation of Gram-Positive and Gram-Negative Bacteria Using Fluorescent Light. *J. Photochem. Photobiol. A Chem.* **2007**, *186*, 335–341. [[CrossRef](#)]
73. Razaq, Z.; Khalid, A.; Ahmad, P.; Farooq, M.; Khandaker, M.U.; Sulieman, A.; Rehman, I.U.; Shakeel, S.; Khan, A. Photocatalytic and Antibacterial Potency of Titanium Dioxide Nanoparticles: A Cost-Effective and Environmentally Friendly Media for Treatment of Air and Wastewater. *Catalysts* **2021**, *11*, 709. [[CrossRef](#)]
74. Ohtani, B.; Prieto-Mahaney, O.O.; Li, D.; Abe, R. What is Degussa (Evonik) P25? Crystalline Composition Analysis, Reconstruction from Isolated Pure Particles and Photocatalytic Activity Test. *J. Photochem. Photobiol. A Chem.* **2010**, *216*, 179–182. [[CrossRef](#)]
75. Zhao, W.; Chen, C.; Li, X.; Zhao, J.; Hidaka, H.; Serpone, N. Photodegradation of Sulforhodamine-B Dye in Platinized Titania Dispersions under Visible Light Irradiation: Influence of Platinum as a Functional Co-catalyst. *J. Phys. Chem. B* **2002**, *106*, 5022–5028. [[CrossRef](#)]
76. Hurum, D.C.; Agrios, A.G.; Gray, K.A.; Rajh, T.; Thurnauer, M.C. Explaining the Enhanced Photocatalytic Activity of Degussa P25 Mixed-Phase TiO₂ Using EPR. *J. Phys. Chem. B* **2003**, *107*, 4545–4549. [[CrossRef](#)]

77. Lu, H.; Zhao, B.; Pan, R.; Yao, J.; Luo, L.; Liu, Y. Safe and Facile Hydrogenation of Commercial Degussa P25 at Room Temperature with Enhanced Photocatalytic Activity. *RSC Adv.* **2014**, *4*, 1128. [[CrossRef](#)]
78. Nuño, M.; Ball, R.; Bowen, C. Photocatalytic Properties of Commercially Available TiO₂ Powders for Pollution Control. In *Semiconductor Photocatalysis—Materials, Mechanisms and Applications*; IntechOpen: London, UK, 2016; p. 613.
79. Sraw, A.; Wanchoo, R.K.; Toor, A.P. Optimization and Kinetic Studies for Degradation of Insecticide Monocrotophos Using LR Grade and P25 TiO₂ under UV/Sunlight Conditions. *Environ. Prog. Sustain. Energy* **2014**, *33*, 1201–1208. [[CrossRef](#)]
80. Brezová, V.; Vrecková, Z.; Billik, P.; Čaplovičová, M.; Plesch, G. Photoactivity of Mechanochemically Prepared Nanoparticulate Titanium Dioxide Investigated by EPR Spectroscopy. *J. Photochem. Photobiol. A Chem.* **2009**, *206*, 177–187. [[CrossRef](#)]
81. Lakshmi, S.; Renganathan, R.; Fujita, S. Study on TiO₂-Mediated Photocatalytic Degradation of Methylene Blue. *J. Photochem. Photobiol. A Chem.* **1995**, *88*, 163–167. [[CrossRef](#)]
82. Fernández-Pérez, A.; Valdés-Solís, T.; Marbán, G. Visible Light Spectroscopic Analysis of Methylene Blue in Water; the Resonance Virtual Equilibrium Hypothesis. *Dye. Pigment.* **2019**, *161*, 448–456. [[CrossRef](#)]
83. Rangel, R.; Cedeño, V.J.; Espino, J.; Bartolo-Pérez, P.; Rodríguez-Gattorno, G.; Alvarado-Gil, J.J. Comparing the Efficiency of N-Doped TiO₂ and N-Doped Bi₂MoO₆ Photo Catalysts for MB and Lignin Photodegradation. *Catalysts* **2018**, *8*, 668. [[CrossRef](#)]